OPEN ACCESS
Journal of Innovative Optical Health Sciences
Vol. 14, No. 1 (2021) 2140007 (11 pages)

DOI: 10.1142/S1793545821400071

World Scientific
www.worldscientific.com

Research on optical properties of cardiovascular tissues based on OCT data

Na Qin, Yana Liu, Lin Huang, Yi Xin, Xiao Zhang,
Xiaoming Hu and Qin Li*
School of Life Science, Beijing Institute of Technology
5 South Zhongguancun Street, Beijing, P. R. China
**liqin@bit.edu.cn*

Received 7 December 2020
Accepted 8 December 2020
Published 9 January 2021

As a high-resolution optical imaging technology, Optical Coherence Tomography (OCT) has been widely used in the diagnosis and treatment of cardiovascular diseases. It has played an important role in the detection and identification of atherosclerotic plaques and has significant advantages. In this paper, we realized to extract the optical characteristic parameters of the target sample based on the OCT data by establishing optical transmission models conforming to the OCT principle. The optical phantoms and coronary artery of domestic pig were used as research samples to study the difference between the optical properties of the cardiovascular tissues. It can provide a basic method for further study of optical characteristic parameters of atherosclerotic plaques, and also lay a foundation for realizing the quantitative evaluation of atherosclerotic plaques with multiple optical characteristic parameters in the future.

Keywords: Optical coherence tomography; optical characteristic parameters; theoretical model of optical transmission; phantoms; coronary artery.

1. Introduction

Atherosclerosis is a disease caused by inflammation of the blood vessel. The formation of plaque is the inducement of coronary heart disease. Its rupture or erosion can lead to thrombosis and subsequent cardiovascular events, which can cause the death of patients.

As the latest emerging imaging technology, optical coherence tomography (OCT)[1] has a wide range of applications in the field of biomedicine, and is gradually being used in clinics. Intravascular optical coherence tomography (IVOCT) combines OCT technology and endoscopes to perform high-resolution tomography of the inner wall of the blood vessel, using near-infrared light.[2] We can observe the morphological and structural information of the blood vessel wall and atherosclerotic plaques. And now, IVOCT plays an important role in the diagnosis and treatment of cardiovascular diseases.

*Corresponding author.

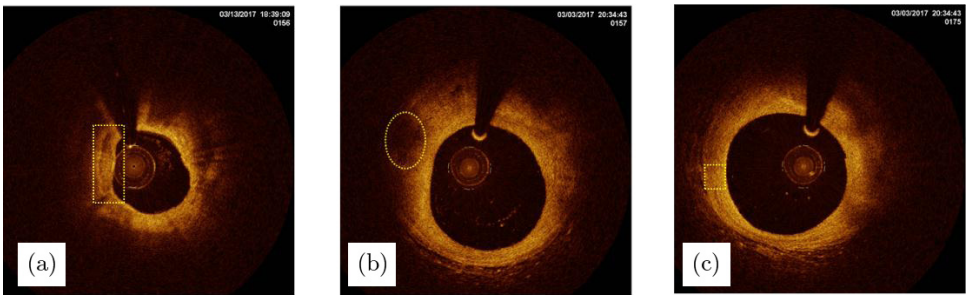

Fig. 1. OCT images of three types of atherosclerotic plaques. (a) Calcified plaque, (b) lipid plaque, and (c) fibrous plaque.

In order to give full play to the advantages of OCT in the detection and evaluation of atherosclerotic plaques, and to improve the clinical value, many researchers have carried out some related researches, mainly including three aspects, namely, the establishment of high-performance OCT system, identification and detection of vulnerable plaques,[3] and assessment of atherosclerotic plaques.[4,5]

At present, it remains at the stage of qualitative evaluation of atherosclerotic plaques based on the OCT image standard of different types of plaques established by Yabushita *et al.*[4] in the clinic. Just as in Fig. 1, OCT images of three main types of atherosclerotic plaques are displayed. Calcified plaques appear as heterogeneous signal-poor regions with sharp delineate borders in the OCT image. Lipid plaques are also signal-poor regions, but they are homogeneous with diffuse delineate borders, while fibrous plaques appear as homogeneous signal-rich regions. The yellow dotted box in Fig. 1 is the corresponding area of three typical plaques in the OCT images which was obtained using the Dragonfly Optis imaging system (LightLab Imaging, St Jude Medical, Minnesota, USA).

Many studies have proposed semi-automatic or automatic identification and classification algorithms of plaques according to this standard to improve work efficiency.[6–9] However, it needs to rely on the experience of clinicians to determine. There are problems such as misdiagnosis or even inability to diagnose due to lack of experience and differences in diagnosis between clinicians. Therefore, quantitative evaluation can provide objective and reliable information of plaques and help improve the accuracy of the diagnosis. In addition to measuring some physical dimensions from the OCT image to describe the plaques,[10,11] we can also use the indicators of the plaque itself to evaluate the atherosclerotic plaque, such as optical characteristic parameters.[12–15]

By now, the qualitative evaluation of plaque type is on its way. The judgement of plaque type is still based on the experience of clinicians. Therefore, it has certain subjectivity and individual evaluation differences. The purpose of this research is to study the differences in optical properties of sample and set up a method to describe the optical characteristics by some parameters, that can be used to quantitatively evaluate the sample properties. By studying the optical properties of optical phantoms and domestic pig coronary arteries, a method for characterizing the optical properties of cardiovascular tissues is established. The work provides a foundation for further research on the optical characteristic parameters of atherosclerotic plaque.

2. Materials and Methods

Figure 2 shows the schematic of the main research content and methods in this paper. The optical characteristic parameters of samples are extracted by establishing theoretical model of optical

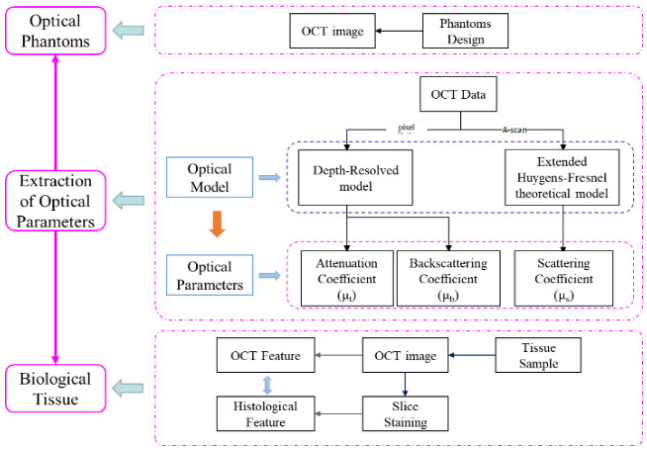

Fig. 2. The schematic of the main research content and methods.

transmission conforming to OCT principle to study the optical properties of cardiovascular tissues.

2.1. *Sample preparation*

In order to study the optical properties of cardiovascular tissues, we selected optical phantoms and actual biological tissues for experiments.

Before conducting experiments on biological tissues, ideal optical phantoms of cardiovascular tissue were fabricated by the casting technology and spin coating technology. We selected polydimethylsiloxane (PDMS) that is commonly used in academic research and industry as the substrate material. PDMS is an optically transparent organic silicon material, of which the refractive index in the near-infrared region is close to that of biological tissues. In addition, we chose inorganic particles of titanium dioxide (TiO_2) and aluminum oxide (Al_2O_3) with strong compatibility and adjustability as the scattering diluent, and the most commonly used carbon black as the absorbent. The materials designed for phantoms are shown in Table 1.

The fabrication of optical phantoms of cardiovascular tissues with different optical properties is achieved by controlling the proportion and concentration of inorganic molecular particles, including phantoms of atherosclerotic plaque with single-layer parallel structure and phantom of coronary artery with multi-layer parallel structure.

Studies have shown that the polymorphism and morphological structure of the domestic pig's coronary artery is very similar to that of human, and it is easy to obtain. Therefore, the coronary artery of domestic pig is selected as the biological sample of cardiovascular tissues.

The coronary artery was peeled off the heart and the peripheral tissues were removed to obtain a certain length of the expanded sample for experiments.

2.2. *Data acquisition*

The sample, phantom or biological tissue, is scanned and imaged with OCT equipment to collect the images and data. The device used in the experiments is a swept source optical coherence tomography (SS-OCT) built by the laboratory, which is mainly composed of light source with a FWHM bandwidth of 70 nm centered at 1310 nm (AXSUN), interferometer, sample arm, reference arm, and data acquisition and processing module. It has a lateral resolution with 11 μm and axial resolution with 13 μm in air. The imaging ranges are 4 mm in the transverse direction and 4.8 mm in the longitudinal direction.

The histological verification is realized by tissue slice staining. Hematoxylin-Eosin (HE) was chosen as the dye and then white-light panoramic scan was performed. Thus, the histological results were obtained to make a comparison with OCT images.

2.3. *Optical parameters extraction*

The specific method flow is shown in Fig. 3. Optical transmission models conforming to the OCT principle were established, for extracting the optical characteristic parameters of the sample based on the OCT data. The models we selected are the extended Huygens–Fresnel (EHF) theoretical model and the Depth-Resolved (DR) model. In the process, the dynamic programming algorithm is used to recognize the region of interest (ROI) of the sample. After extraction, the attenuation coefficient (μ_t), scattering coefficient (μ_s), and backscattering coefficient (μ_b) that characterize the optical properties of the sample are finally obtained. The parts of (a), (b), (c), and (d) in Fig. 3 show the schematic flow diagram of the EHF theoretical model.

2.3.1. *EHF theoretical model*

The EHF theoretical model,[16] taking the contribution of multiple scattered photons to the OCT

Table 1. The materials of optical phantoms.

Category	Name	Brand	Type	Specification
Substrate material	PDMS	Dow Corning	SYLGARD^{TM} 184	/
Scattering	TiO_2	RHAWN	Anatase	2–3 μm
diluent	Al_2O_3	RHAWN	α-crystal	200 nm
Absorbent	Carbon Black	CABOT	VULCAN XC72	30 nm

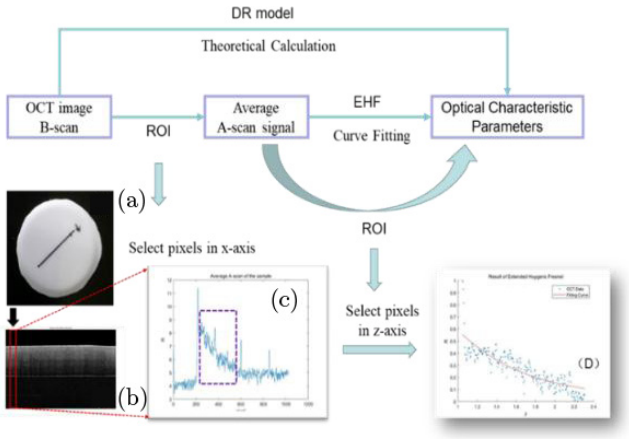

Fig. 3. Flowchart of optical characteristic parameters extraction.

signal into consideration, expresses the OCT signal based on the depth distribution is a function related to the scattering coefficient, anisotropy factor, and other parameters.[17] The mean square of the heterodyne current signal $I^2(z)$ at the depth z measured by the OCT system is the product of two factors as follows:

$$\langle I^2(z)\rangle = \langle i^2\rangle_0 \psi(z). \tag{1}$$

Here, $\psi(z)$ is the heterodyne efficiency factor describing the signal degradation caused by scattering, which contains scattering effects. The formula shows that

$$\psi(z) = \exp(-2\mu_s z) + [1-\exp(-\mu_s z)]^2 \frac{\omega_H^2}{\omega_S^2} + \frac{4\exp(-\mu_s z)[1-\exp(-\mu_s z)]}{1+\omega_S^2/\omega_H^2}. \tag{2}$$

In Eq. (2), the first term represents the contribution of the single scattered photon to the OCT signal, while the second term represents the contribution of multiple scattered photons. The third term in Eq. (2) is a cross-term including both single scattering contribution and multiple scattering contribution. ω_H and ω_S represent the radius at $1/e$ irradiance radius at the probing depth without or with scattering, respectively.[17]

$$\omega_H^2 = \omega_0^2\left(A - \frac{B}{f}\right)^2 + \left(\frac{B}{k\omega_0}\right)^2, \tag{3}$$

$$\omega_S^2 = \omega_0^2\left(A - \frac{B}{f}\right)^2 + \left(\frac{B}{k\omega_0}\right)^2 + \left(\frac{2B}{k\rho_0(z)}\right)^2, \tag{4}$$

where A and B are elements in the ABCD ray-matrix, which is used to describe the process of light propagation from the lens plane to the sample.[18] When the focal plane of the sample beam is fixed on the internal interface of the sample, $A=1$ and $B=f$, while, $A=1$ and $B=f+z/n$ when the focal plane is fixed on the surface. ω_0 represents the $-1/e$ irradiance radius of the input sample beam at the lens plane, $k=2\pi/\lambda$. $\rho_0(z)$ in Eq. (4) is the lateral coherence length, and the derived formula is as follows:

$$\rho_0(z) = \sqrt{\frac{3}{\mu_s z}}\frac{\lambda}{\pi\theta_{\text{rms}}}\left(\frac{nB}{z}\right). \tag{5}$$

In the above formula, θ_{rms} represents the root-mean-square scattering angle, which is defined as the half-width at $1/e$ of the maximum of the Gaussian curve in accordance with the main frontal lobe of the scattering phase function, and the relationship with the effective anisotropy factor is $g_{\text{eff}} = \cos\theta_{\text{rms}}$. θ_{rms} and scattering coefficient μ_s are both fitting parameters which can be obtained simultaneously through data fitting in the EHF theoretical model.

Select the ROI from the OCT image, and evenly extract the adjacent A-scan signal along the horizontal direction for averaging. Choose the number of vertical pixels to be fitted in the average A-scan signal, which must ensure that the selected pixels are all image information corresponding to the sample tissue. Using the fitting algorithm composed of Eqs. (2) to (5) for fitting, the fitting parameters μ_s and g_{eff} can be obtained.

2.3.2. *DR model*

The DR model is a new OCT transmission theoretical model proposed in recent years to calculate the attenuation coefficient of each pixel in the OCT image. According to the introduction of Vermeer *et al.*,[19] the digital signal detected at depth z, $I(z)$ shows that

$$I(z) \cong \beta \cdot L_0 \cdot \mu_b(z) \cdot e^{-2\int_0^d \mu_t(u)du}, \tag{6}$$

where β represents both the quantum efficiency of the detector and the converting factor of the digitizer,[20] L_0 is the power of the light source (Wm^{-2}), μ_t and μ_b are the attenuation coefficient and backscattering coefficient, respectively.

As we all know, backscattered light is a part of scattered light which is a part of attenuated light. Thus, backscattered light is a part of attenuated

light and its propagation direction is opposite to the original direction. Let $\mu_b(z) = \alpha\mu_t(z)$ perform the equivalent substitution to the above equation and then integrate from z to infinity, the ratio of Eq. (6) to the result is the estimated attenuation, as shown in Eq. (7).

$$\mu_t(z) \cong \frac{I(z)}{2\int_z^{\infty} I_b(u)du}. \tag{7}$$

Furthermore, the attenuation coefficient obtained according to the OCT image intensity is

$$\mu[i,j] \cong \frac{I[i,j]}{2\Delta\sum_{y=j+1}^{\infty} I[i,j]}. \tag{8}$$

Here, the OCT image intensity is expressed as a matrix $I[i,j]$ of size $M \times N$, i and j represent the number (pixel) of A-scan and depth, respectively, Δ is the size of pixel in the OCT image (mm/pixel).

The model is further extended to estimate the backscatter term: assume that the depth coordinates in the uniform area start at z_1 and end at z_2, thus, we believe that the attenuation coefficient and backscattering coefficient at each depth $z \in (z_1, z_2)$ are all the same, that is, $\mu_t(z) = \tilde{\mu}_t$ and $\mu_b(z) = \tilde{\mu}_b$, so Eq. (6) can be simplified to the following formula:

$$I(z) \cong L' \cdot \tilde{\mu}_b \cdot e^{-2\cdot r\cdot\tilde{\mu}_t}, \tag{9}$$

where $r = z - z_1$ and $r \in [0, z_2 - z_1]$. The formula $L'\beta = L_0 \cdot e^{-2\int_0^{z_1}\mu_t(u)du}$ is the reduced light intensity along the path from the catheter to the designated area,[20] L' is the reduced optical power at the depth z_1, which has the same unit as L_0.

We define z_1 and z_2 as the beginning and end of a pixel, then $e^{-2\cdot r\cdot\tilde{\mu}_t}$ is approximately 1 because r is very small. Divide Eq. (10) by the factor $e^{-2\int_0^{z_1}\mu_t(u)du}$ and take the logarithm to get the approximate value of the backscatter term:

$$T_b(z) = \ln\frac{L_0}{\beta}\cdot\tilde{\mu}_b \cong \ln I_b(z) + 2\int_0^{d_1}\tilde{\mu}_t(u)du, \tag{10}$$

where $\tilde{\mu}_t(u)$ is the estimated attenuation at depth u. The definition term $T_b(z)$ is linearly related to the logarithm of the backscattering coefficient and has a constant offset related to the initial incident energy L_0 and the imaging parameter β. According to this, we get the backscattering coefficient μ_b as follows:

$$\mu_b[i,j] \approx \frac{\ln I[i,j] + 2\Delta\sum_{y=1}^{j} I[i,y]}{\ln\frac{L_0}{\beta}}. \tag{11}$$

According to Eqs. (8) and (11), the attenuation coefficient and backscattering coefficient corresponding to each pixel can be calculated point by point, and stored in a two-dimensional matrix.

2.4. *Statistical analysis*

SPSS (Statistical Product and Service Solutions) was used to perform statistical analysis on the optical characteristic parameters of different samples. Univariate of the general linear model was selected to compare them pairwise to obtain the descriptive statistics and homogeneity tests. And then the statistical results were described.

3. Experiments and Implementation

There are two parts for the experiments, including optical phantoms and biological tissue in this section. Prepare the samples respectively, and then extract the optical characteristic parameters based on the OCT data so as to study the differences of optical properties between different structures.

3.1. *Phantoms design*

Ideal parallel phantoms for experiments were fabricated using spin coater, including single-layer phantoms of atherosclerotic plaque and multi-layer phantom of coronary artery. In order to be as close to the actual biological tissue as possible, the preparation ratio of this section refers to that in the literatures.[21,22]

The substrate material PDMS for the plaque phantoms with single-layer parallel structure is 10 mL and the ratio of the two groups is 10:1. The detailed proportioning information of the scattering diluent and the absorbent is shown in Table 2.

Tables 3 and 4 show the results of optical characteristic parameters of plaque phantoms. The values are given in the form of mean ± standard deviation (mean ± std). Lipid phantom has the characteristics of strong backscattering and strong attenuation; calcified phantom has weak backscattering and attenuation; fibrous phantom has the characteristics of strong backscattering and weak attenuation. It can be seen that the optical characteristic parameters between different types of plaque phantoms presented by the table data

Table 2. The prepared proportion of single-layer parallel phantoms of plaques.

Types of phantoms	Number	Scattering particle	Concentration of scattering diluent (mg/mL)	Concentration of absorbent (mg/mL)	Thickness (mm)
Lipid	A1	Al_2O_3	20	0.8	0.70
	A2	TiO_2			0.60
Calcified	B1	Al_2O_3	5	15	0.50
	B2	TiO_2			0.78
Fibrous	C1	Al_2O_3	20	/	0.44
	C2	TiO_2			0.60

Table 3. Results of optical characteristic parameters of plaque phantoms with Al_2O_3 as a scattering diluent.

Serial number Type	A1 Lipid_Al	B1 Calcified_Al	C1 Fibrous_Al
μ_t	17.8248 ± 4.7712	17.9720 ± 7.6143	15.0350 ± 6.7037
μ_s	3.1818 ± 3.0901	3.2655 ± 3.2401	3.1328 ± 2.8159
μ_b	0.8546 ± 0.0735	0.8599 ± 0.1009	0.8614 ± 0.0919

Table 4. Results of optical characteristic parameters of plaque phantoms with TiO_2 as a scattering diluent.

Serial number Type	A2 Lipid_Ti	B2 Calcified_Ti	C2 Fibrous_Ti
μ_t	15.9754 ± 4.2921	9.6713 ± 6.6322	9.1979 ± 3.1411
μ_s	2.2295 ± 1.7297	2.7192 ± 2.0534	2.0103 ± 1.9712
μ_b	0.9145 ± 0.0819	0.7627 ± 0.1193	0.8375 ± 0.0627

conform to the optical properties of the plaques to a certain extent.

Previous research[23] has shown that the attenuation coefficient of atherosclerotic plaques obtained from OCT data with a light source of which center wavelength is 1300 nm between 11 and 20 mm^{-1}. Comparing the results of the optical characteristic parameters found that using Al_2O_3 particle as the scattering diluent is closer to the characteristics of cardiovascular tissues. On the other hand, in the literatures[21,22] they also chose Al_2O_3 particle as the scattering diluent to fabricate the phantoms of blood vessel structure. And compared to TiO_2, Al_2O_3 has a lower viscosity so it is easier to be compatible with PDMS, that is, it is easy to prepare a phantom with uniform texture using Al_2O_3.

Therefore, Al_2O_3 is used as the only scattering diluent when preparing the multi-layer phantom, which is arterial phantom with three-layer parallel structure. According to the preparation ratio in the literature, the detailed proportioning information is shown in Table 5. Figure 4 shows the sample of cardiovascular phantoms. They are plaque phantoms with single-layer parallel structure and arterial phantom with three-layer parallel structure.

Table 5. The prepared proportion of three-layer parallel phantom of artery.

Layer	Types of structure	Concentration of scattering diluent	Concentration of absorbent
1	intima	20 mg/mL	/
2	media	14 mg/mL	0.5 mg/mL
3	adventitia	60 mg/mL	/

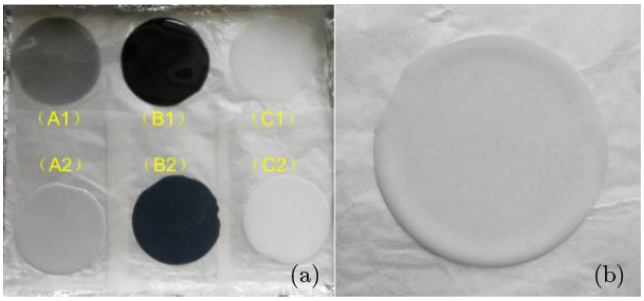

Fig. 4. The sample of arterial phantoms with three-layer parallel structure. (a) Sample of plaque phantoms. (b) Sample of arterial phantom.

3.2. *Tissue anatomy*

The sample of porcine heart was ordered in the supermarket. The porcine heart was taken from the domestic pig slaughtered in the early morning of the same day and sent to the supermarket without freezing. The coronary arteries were taken out as soon as possible after we got the sample in time.

The preparation process is shown in Fig. 5. Figure 5(a) shows the porcine heart, and it is easy to observe the aortic ostium. There are two luminal openings thereby (marked by the red circle), which are starting point of the left and right coronary arteries, respectively. Since the experimental OCT is planar scanning, the tubular coronary artery sample needs to be sectioned radially to facilitate OCT imaging, and then to be placed in physiological saline for use. After taking the OCT images, coronary artery sample were placed into 4% paraformaldehyde for fixation immediately, in support of the tissue slice staining for histological verification. In order to shorten the operation time and keep the samples fresh, all of the operation steps were arranged very compact during the whole experiment process.

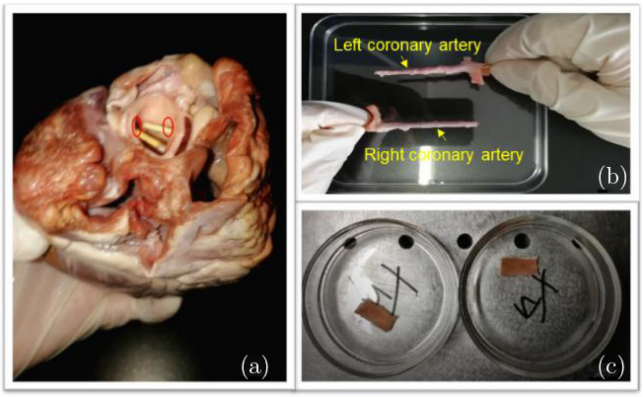

Fig. 5. The preparation process of coronary artery of domestic pig. (a) The porcine heart. (Red circle: the starting point of coronary artery.) (b) Tubular coronary artery after peeling and removing peripheral tissues. (c) Flattened coronary artery after dissection.

4. Results and Discussion

4.1. *Optical phantoms*

Figure 6 is the OCT images corresponding to different plaque phantoms. The OCT image signal of the fibrous plaque phantom is relatively strong. Calcified plaque phantom and lipid plaque phantom are regions with lower signal intensity, however, the former has relatively clear border and that of the latter is more blurred. The results of OCT images are consistent with the image characteristics of the atherosclerotic plaque.

The statistical analysis result is shown in Fig. 7 for optical characteristic parameters of plaque phantoms fabricated by different scattering diluent. The meanings of the letters involved in the abscissa in Fig. 7 are that: ut, us, and ub respectively represent the attenuation coefficient, the scattering coefficient, and the back-scattering coefficient; C, F, and L represent the calcified, fibrous, and lipid plaque phantoms, respectively; Al and Ti represent the scattering diluents Al_2O_3 or TiO_2 particles. That is, Figs. 7(a), 7(c), and 7(e) are the statistical analysis results of the optical characteristic parameters of calcified, fibrous, and lipid plaque phantoms prepared by Al_2O_3 as the scattering diluent. Similarly, Figs. 7(b), 7(d), and 7(f) are the statistical analysis results of the attenuation coefficient, scattering coefficient, and backscattering coefficient of the three plaque phantoms when TiO_2 is used as the scattering diluent.

In Fig. 7, $p < 0.01$ indicates that there is a significant difference between the two. The results show that whether the scattering diluent is Al_2O_3 or TiO_2, the attenuation coefficients, scattering coefficients, and backscattering coefficients of lipid, calcified, and fibrous plaque phantoms all have significant differences.

The OCT image of the arterial phantom is shown in Fig. 8(a). The three-layer bright-dark-bright parallel structure can be clearly seen, which conforms to the OCT image characteristics of the structure of arterial vessel. And Fig. 8(b) is the result of recognition of the phantom by dynamic

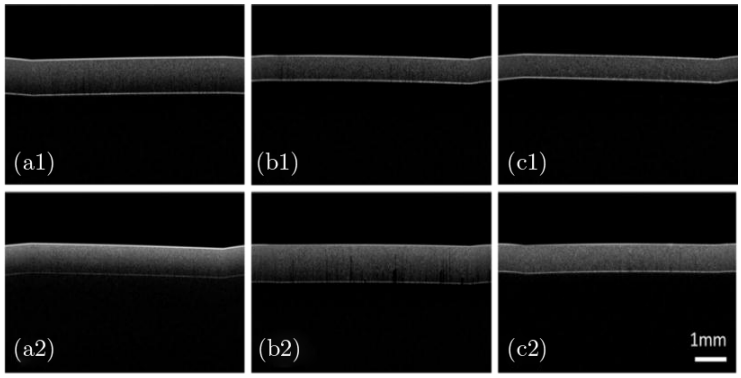

Fig. 6. OCT images of plaque phantoms. (a1)–(c1) Lipid, calcified and fibrous plaque phantom with Al_2O_3 as a scattering diluent. (a2)–(c2) Lipid, calcified and fibrous plaque phantom with TiO_2 as a scattering diluent.

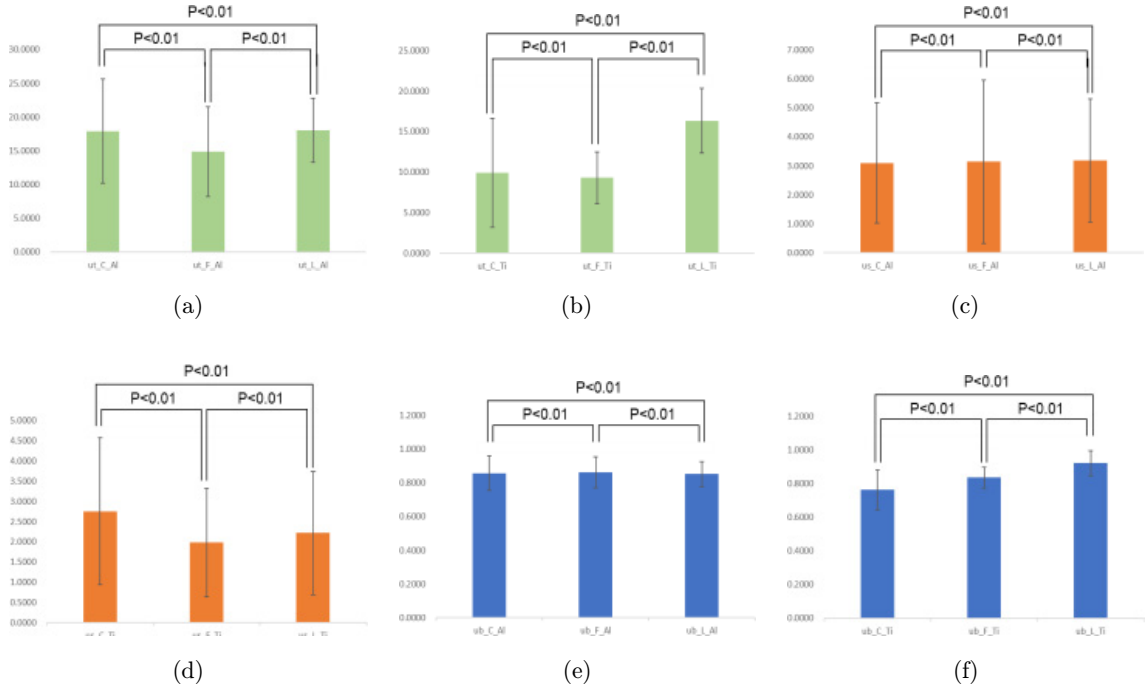

Fig. 7. The results of statistical analysis of the optical characteristic parameters of the plaque phantoms. ($P < 0.01$ have significant differences.)

programming algorithm, in which the boundary lines are marked with lines in different colors.

The optical characteristic parameters of the three-layer structure of the arterial phantom, that are intima, media, and adventitia respectively, are distributed in a certain interval, and there are differences between different structures. For example, the differences of backscattering coefficient between the adventitia and the other two layers are greater than that between the intima and media, while the attenuation coefficient of the media is smaller compared with that of the intima and adventitia. Even though the differences are not significant, comprehensive consideration of the differences among multiple optical characteristic parameters can improve the discrimination among different structures.

The statistical analysis of the optical characteristic parameters of the arterial phantom, as shown in Fig. 9, contains the statistical differences of the optical characteristic parameters of the three-layer structure of arterial phantom, namely the intima, the media, and the adventitia. In Fig. 9, $p < 0.01$ indicates that there is a significant difference

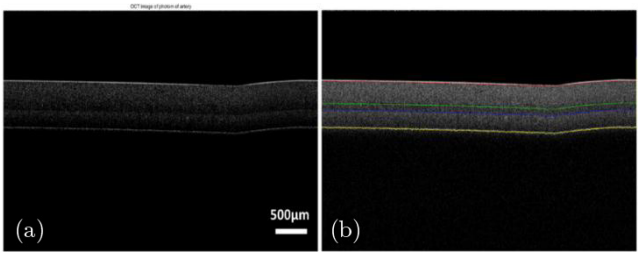

Fig. 8. OCT image of arterial phantom. (a) Original OCT image. (b) Structure recognition by dynamic programming algorithm.

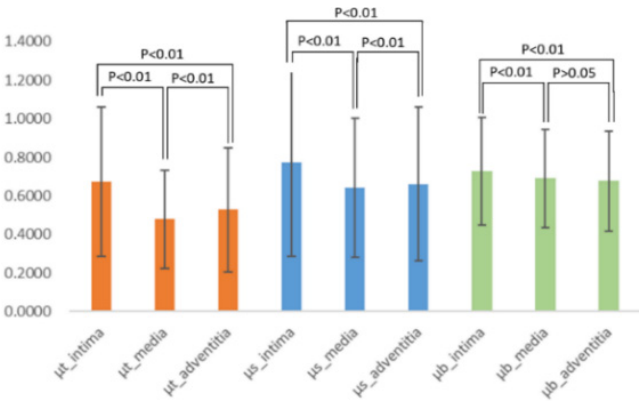

Fig. 9. The statistical analysis results of the optical characteristic parameters of the arterial phantom.

between the two, and $p > 0.05$ indicates that there is no significant difference between the two. The result shows that the intima, media, and adventitia of the arterial phantom all have significant differences in the attenuation coefficient and scattering coefficient. But for the backscattering coefficient, there are significant differences between the intima and the other two, while there is no significant difference between the media and adventitia.

4.2. *Biological tissue*

The optical signals of the intima and adventitia of the coronary artery are stronger than that of the media, because they contain more collagen fibers than the media thus their ability of backscattering is stronger than the media composed of smooth muscle cells. Therefore, the three-layer structure of normal coronary artery can be clearly seen in the IVOCT image. The main manifestations are: the intima and adventitia are high-brightness areas, the media is a low-brightness dark zone, and the overall

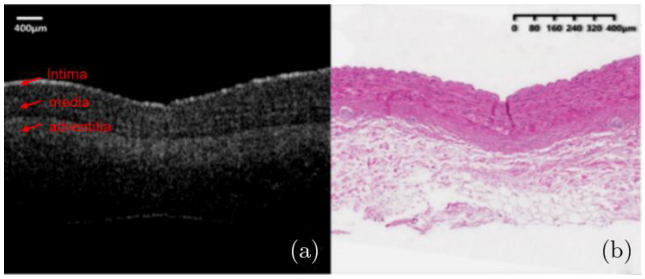

Fig. 10. The result of comparison of OCT image and corresponding histological image. (a) OCT image. (b) The image of corresponding histological result.

appearance is bright-dark-bright IVOCT image characteristics.

Figure 10 is the result of comparison of OCT image and corresponding histological image. As Fig. 10(a) shows, it can be clearly seen that the layered structure of coronary artery, the corresponding three-layer structure presents bright-dark-bright image features. The morphology can be clearly observed, that is, three types of cells can be seen in a layered distribution, just as shown in Fig. 10(b). The first layer from top to bottom is endothelial cells, a thin layer flattened epithelial cells, corresponding to the intima of the coronary artery. The second layer is smooth muscle cells with a long spindle-shaped nucleus and many organelles in the plasma on both sides of the nucleus, the size of which depends on the functional morphology, that is corresponding to the media. The third layer is connective tissue corresponding to the adventitia, which contains a large amount of intercellular substance. There are many types of cells but few in number in the intercellular substance, irregularly arranged and scattered with no polarity. Therefore, there is a good agreement between OCT image and histology.

The dynamic programming algorithm is used to identify the structural layer between different tissues in the OCT image. Just as shown in Fig. 11, the boundary of each layer of tissue structure is marked with a line in different color. The thickness of different tissue structure is calculated as shown in the middle column of Table 6, and the values are given in the form of mean ± std. The last column is the reference value of the actual thickness measured from the histological result of the coronary artery. It proves that the thickness obtained by the dynamic programming algorithm are almost consistent with the actual thickness.

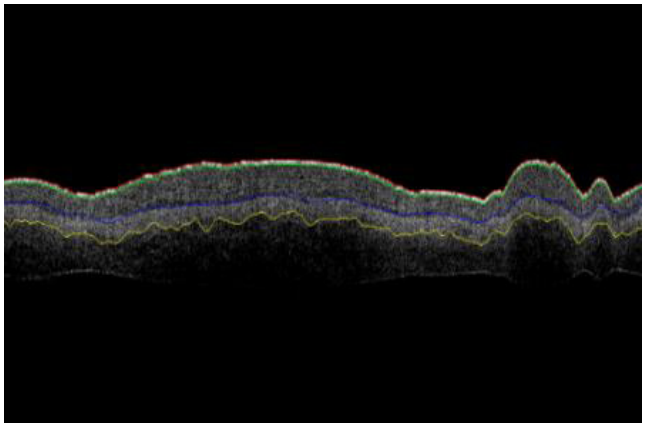

Fig. 11. Schematic diagram of the structural layer of the coronary artery identified by dynamic programming algorithm.

Table 6. The thickness of each layer of coronary artery of porcine heart.

Layer structure	Thickness (μm)	Reference value (μm)
Intima	42.2535 ± 1.4215	41.41
Media	253.8952 ± 64.9755	200.19
Adventitia	180.7690 ± 22.6146	127.06

For each optical characteristic parameter, the values of different vascular structures are distributed within a certain range and have slight differences between each other. Statistical analysis is performed and the result is shown in Fig. 12. It shows that the attenuation coefficient and scattering coefficient of the intima, media, and adventitia of the coronary artery are significantly different, and the backscattering coefficient of the intima are significantly different from that of the media and adventitia. Only there is no significant difference in backscattering coefficient between the media and adventitia. This result is consistent with the experimental result of the aforementioned arterial phantom.

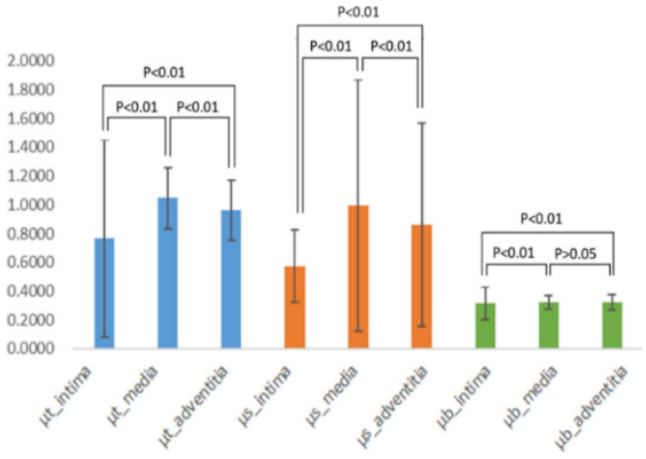

Fig. 12. The statistical analysis results of the optical characteristic parameters of coronary artery of porcine heart.

5. Conclusion

By studying the optical properties of optical phantoms and domestic pig coronary artery, a method for characterizing the optical properties of cardiovascular tissues is proposed. The method is the foundation for further research on the optical characteristic parameters of atherosclerotic plaque. The ultimate aim of this research is to study the optical property differences in different types of atherosclerotic plaques based on original OCT data, in order to quantitatively evaluate atherosclerotic plaques based on the optical characteristic parameters.

The method set up in this research can directly transfer to the analysis of atherosclerotic plaques. The dynamic programming algorithm is used to realize the automatic recognition of the sample based on the OCT image, that is, identify the area boundary of the same tissue structure, so as to study optical properties in a targeted ROI; the optical characteristic parameters, including attenuation coefficient, scattering coefficient, and backscattering coefficient of samples, are extracted from OCT data by the EHF theoretical model and DR model. The phantom of atherosclerotic plaque can be used to verify the rationality and validity of the theoretical model and make the model more reasonable. The structure of blood vessel is determined by comparison between OCT image and histological result. And then, the optical characteristic parameters of the blood vessel and plaques are extracted from original OCT data. The difference between the blood vessel and plaques can be displayed by the multiple parameters so that further quantitative identification of atherosclerotic plaque is realized according to the optical characteristic parameters. The comprehensive consideration of multiple optical characteristics of the plaques ensures the reliability of the artificial intelligence recognition system. And plaque identification can be more objective without relying on the experience of clinicians.

Conflicts of Interest

The authors declare that there are no conflicts of interest relevant to this paper.

Acknowledgments

This work was supported by the National Natural Science Foundation of China (61975017, 61905015).

References

1. D. Huang, E. A. Swanson, C. P. Lin *et al.*, "Optical coherence tomography," *Science* **254**(5035), 1178–1181 (1991).
2. M. E. Brezinski, G. J. Tearney, B. E. Bouma *et al.*, "Imaging of coronary artery microstructure (in vitro) with optical coherence tomography," *Am. J. Cardiol.* **77**(1), 92–93 (1996).
3. A. P. Burke, A. Farb, G. T. Malcom *et al.*, "Coronary risk factors and plaque morphology in men with coronary disease who died suddenly," *New Engl. J. Med.* **336**(18), 1276–1282 (1997).
4. H. Yabushita, B. E. Bouma, S. L. Houser *et al.*, "Characterization of human atherosclerosis by optical coherence tomography," *Circulation* **106**(13), 1640–1645 (2002).
5. C. Xu, J. M. Schmitt, S. G. Carlier *et al.*, "Characterization of atherosclerosis plaques by measuring both backscattering and attenuation coefficients in optical coherence tomography," *J. Biomed. Opt.* **13**(3), 034003 (2008).
6. G. J. Ughi, T. Adriaenssens, P. Sinnaeve *et al.*, "Automated tissue characterization of in vivo atherosclerotic plaques by intravascular optical coherence tomography images," *Biomed. Opt. Exp.* **4**(7), 1014–1030 (2013).
7. L. S. Athanasiou, C. V. Bourantas, G. Rigas *et al.*, "Methodology for fully automated segmentation and plaque characterization in intracoronary optical coherence tomography images," *J. Biomed. Opt.* **19**(2), 026009 (2014).
8. M. Xu, J. Cheng, D. W. K. Wong *et al.*, "Automatic image classification in intravascular optical coherence tomography images," *Proc. TENCON 2016 - 2016 IEEE Region 10 Conf.* (Singapore, 2016), pp. 1544–1547.
9. N. Gessert, M. Heyder, S. Latus *et al.*, "Adversarial training for patient-independent feature learning with IVOCT data for plaque classification" (2018), arXiv:1805.06223.
10. E. Mehanna, H. G. Bezerra, D. Prabhu *et al.*, "Volumetric characterization of human coronary calcification by frequency-domain optical coherence tomography," *Circ. J.* **77**(9), 2334–2340 (2013).
11. A. Fujino, G. Mintz, M. Matsumura *et al.*, "A new optical coherence tomography-based calcium scoring system to predict stent under-expansion," *J. Am. College Cardiol.* **70**(18), B12-B3 (2018).
12. S. G. Van, T. Goderie, E. Regar *et al.*, "Atherosclerotic tissue characterization in vivo by optical coherence tomography attenuation imaging," *J. Biomed. Opt.* **15**(1), 011105 (2010).
13. W. C. Kuo, M. W. Hsiung, J. J. Shyu *et al.*, "Assessment of arterial characteristics in human atherosclerosis by extracting optical properties from polarization-sensitive optical coherence tomography," *Opt. Exp.* **16**(11), 8117–8125 (2008).
14. J. M. Schmitt, A. Knuttel, M. Yadlowsky *et al.*, "Optical-coherence tomography of a dense tissue: Statistics of attenuation and backscattering," *Phys. Med. Biol.* **39**(10), 1705–1720 (1994).
15. G. T. Smith, N. Dwork, D. O'connor *et al.*, "Depth-resolved estimation of the attenuation coefficient from optical coherence tomography data," *IEEE Trans. Med. Imaging* **34**(12), 2592–2602 (2015).
16. L. Thrane, H. T. Yura, P. E. Andersen, "Analysis of optical coherence tomography systems based on the extended Huygens-Fresnel principle," *J. Opt. Soc. Am. A* **17**(3), 484–490 (2000).
17. C. C. Cheng, M. G. Raymer, "Propagation of transverse optical coherence in random multiple-scattering media," *Phys. Rev. A* **62**, 1–12 (2000).
18. H. T. Yura, S. G. Hanson, "Optical beam wave propagation through complex optical systems," *J. Opt. Soc. Am. A* **4**(10), 1931–1948 (1987).
19. K. A. Vermeer, J. Mo, J. J. A. Weda *et al.*, "Depth-resolved model-based reconstruction of attenuation coefficients in optical coherence tomography," *Biomed. Opt. Exp.* **5**(1), 322–337 (2013).
20. S. Liu, Y. Sotomi, J. Eggermont *et al.*, "Tissue characterization with depth-resolved attenuation coefficient and backscatter term in intravascular optical coherence tomography images," *J. Biomed. Opt.* **22**(9), 1–16 (2017).
21. C.-E. Bisaillon, M. L. Dufour *et al.*, "Artery phantoms for intravascular optical coherence tomography: Healthy arteries," *Biomed. Opt. Exp.* **2**(9), 2599–2613 (2011).
22. C.-E. Bisaillon, G. Lamouche, "Artery phantoms for intravascular optical coherence tomography: Diseased arteries," *J. Biomed. Opt.* **18**(9), 6010 (2013).
23. G. Lamouche, B. F. Kennedy, K. M. Kennedy *et al.*, "Review of tissue simulating phantoms with controllable optical, mechanical and structural properties for use in optical coherence tomography," *Biomed. Opt. Exp.* **3**(6), 1381–1398 (2012).